Received: 14 September 2024 | Revised: 8 November 2024 | Accepted: 2 December 2024

IET Electric Power Applications

DOI: 10.1049/elp2.12530

The Institution of Engineering and Technology WILEY

ORIGINAL RESEARCH

Hybrid mechanism-data-driven iron loss modelling for permanent magnet synchronous motors considering multiphysics coupling effects

Lin Liu[1] | Wenliang Yin[2] | Youguang Guo[1]

[1]School of Electrical and Data Engineering, University of Technology Sydney, Ultimo, New South Wales, Australia

[2]School of Electrical and Computer Engineering, The University of Sydney, Darlington, New South Wales, Australia

Correspondence

Lin Liu.
Email: lin.liu@student.uts.edu.au

Funding information

China Scholarship Council, Grant/Award Number: 201906730038; Australian Research Council, Grant/Award Numbers: DP120104305, DP180100470; National Natural Science Foundation of China, Grant/Award Number: 52005306

Abstract

The precise calculation of iron losses in permanent magnet synchronous motors (PMSMs) remains challenging due to the interplay between various disciplines such as electromagnetism, magnetism, and thermal/mechanical dynamics. Purely mechanistic models require detailed theoretical knowledge and exact parameters, often struggling to accurately describe complex systems, while purely data-driven methods lack interpretability, which are susceptible to data noise and outliers in feature extraction and complicated pattern recognition. Consequently, this paper aims to present a hybrid mechanism-data-driven model for accurately estimating the iron loss for PMSMs, considering the multiphysics coupling effects. Specifically, based on the well-defined physical principles, an advanced iron loss analytical model that simultaneously considers mechanical stress, temperature rise, harmonics, load currents, and changing frequency is developed and then utilised to calculate numerous loss data under different operating conditions, providing a certain level of stability and reliability for prediction accuracy. Subsequently, a convolutional neural network (CNN) algorithm is employed to perform deep learning to extract features and patterns from the data. By defining a suitable loss function, the pre-trained model was fine-tuned and optimised using a small amount of actual data. To validate its superiority, extensive numerical and experimental analyses are conducted on the prototype. The results demonstrate that the iron losses computed using this hybrid model overcome the limitations of singular methods by effectively leveraging both theoretical knowledge and real-world data, thus accurately accommodating various application scenarios. This integrated approach enhances the accuracy, stability, and interpretability of the model, laying a solid foundation for more specialised applications in the future.

KEYWORDS

data analysis, electromagnetic coupling, genetic algorithms, losses, permanent magnet motors

1 | INTRODUCTION

Permanent magnet synchronous motors (PMSMs) are renowned for their high efficiency and power density, which are widely utilised in various fields such as electric vehicles, aerospace, and industrial automation. In these applications, energy conservation and emission reduction are of paramount importance. Accurate calculation of iron losses can optimise motor design and operation, enhance overall system efficiency, reduce energy waste, and thus meet the requirements for high efficiency energy conservation [1, 2]. However, calculating the iron losses of PMSMs involves knowledge from multidisciplinary fields. It requires comprehensive considerations of factors such as material characteristics, electromagnetic field distribution,

temperature effects, and mechanical stress [3, 4]. Establishing an accurate multi-physics coupling model is a key challenge in calculating the iron losses for PMSMs.

Before big data rising, scientists and engineers have conducted extensive and in-depth research on the precise modelling of iron losses. A variety of methods, such as the classical loss models [5], hysteresis models [6, 7], finite element models (FEMs) [8–10], frequency domain models [11, 12], temperature dependency models [13], and empirical models [14] were developed for accurate iron loss calculations. These studies provided significant theoretical foundations and practical tools for understanding and predicting iron losses, playing a crucial role in the design and optimisation of motors, power transformers, and other electromagnetic devices. However, as the complex nature of iron loss mechanisms involves multiple disciplines, each technique has its advantages and limitations in iron loss modelling.

For instance, classical loss models are suitable for sinusoidal excitation but lack accuracy for complex waveforms and non-sinusoidal conditions. Moreover, they cannot accurately account for the non-linear properties of magnetic materials. While hysteresis models and temperature dependency modelling methods can simulate material characteristics, they increase the complexity of determining model parameters. FEMs and frequency domain models can effectively mitigate these issues but they require significant computational resources and time. Starting from the perspective of electric machines, empirical models are typically developed based on a specific dataset and may not be able to extrapolate well to new unseen data. This can lead to inaccurate predictions when the model is applied to materials or conditions that are outside the range of the training data. In summary, although the aforementioned traditional or improved modelling methods can accurately describe iron losses to a certain extent, errors still exist in practical applications. By leveraging the strengths of different methods, it is possible to establish a comprehensive model that enhances the accuracy, efficiency and applicability.

Recently, machine learning techniques have made significant strides, with deep neural networks achieving cutting-edge breakthroughs in fields such as computer vision, natural language processing, speech processing, and reinforcement learning [15, 16]. Neural networks' flexibility, scalability, and deep abstraction/representation capabilities enable their seamless application across domains with sufficient data, inspiring researchers to tackle scientific problems like physical system modelling [17, 18]. For electrical machines, in Ref. [19], the authors proposed a novel physics-informed neural network-based high-frequency modelling method for induction motors offering high accuracy, versatility, and simple parameterisation. The proposed model's symmetric circuit structure enables its applicability to both star- and delta-connected motors without recalculating circuit element values. In Ref. [20], the authors of the work proposed using deep neural networks to predict temperatures inside PMSMs, eliminating the need for thermal modelling expertise. The approach achieves strong performance with minimal model sizes comparable to classic methods. Ortombina et al. proposed using radial basis function neural networks to model complex motor relationships capturing non-linearity and cross-coupling effects. The network takes voltages and currents as inputs and returns flux linkages as output, enabling accurate model-based control in Ref. [21]. Similarly, in Ref. [22], the authors of the paper presented a novel artificial neural network surrogate model for the transient simulation of induction machines. The model is trained using finite element data and can accurately estimate current and torque in real time based on voltage and measured shaft speed inputs. Despite the remarkable progress made by statistical machine learning models in reducing modelling complexity and improving prediction accuracy with the aid of big data, many limitations still exist when deploying these purely data-driven models in real-world applications. For example, predictions may lack robustness, suffer from a lack of interpretability, and potentially violate physical constraints or common sense.

In this case, the hybrid mechanism-data-driven model, integrating the feature extraction prowess of deep learning frameworks with the modelling rigour of conventional physics-based methodologies, exhibits immense potential in tackling intricate physical modelling challenges, particularly in the realm of structural health monitoring and disease diagnosis and prognosis [23–25]. Despite its widespread success across diverse disciplines, its application to iron loss modelling remains relatively nascent. On the other hand, the complexity of iron loss modelling in PMSMs stems from multifaceted sources: Firstly, it encapsulates intricate physical phenomena, including the intricate distribution of magnetic fields and magnetisation states within the motor's architecture. Secondly, the non-linear magnetisation characteristics of the iron core material introduce a non-linear relationship between iron loss and magnetic field intensity, complicating predictive modelling. Furthermore, iron loss varies significantly under different operational conditions, such as varying rotational speeds, loads, and temperatures, necessitating models that can accommodate such dynamicity. Lastly, experimental constraints and costs often hinder the acquisition of extensive, high-quality datasets, posing an additional challenge in robust modelling. Collectively, these factors underscore the suitability of hybrid methods for iron loss modelling in PMSMs. Hybrid methods combining machine learning and physics-informed modelling offer a promising approach to enhance efficiency and accuracy, advancing the state-of-the-art in this critical area of research.

Therefore, considering the complexity of calculating iron losses in PMSMs, influenced by multiple disciplines, this paper first presents an enhanced iron loss analysis model for predicting the iron loss data of PMSMs under various operating conditions. This dataset is utilised to train a convolutional neural network (CNN), which is designed to capture the intricate characteristics of iron loss processes. Moreover, given the practical challenges in acquiring vast amounts of real-world iron loss data due to costs and difficulties, a hybrid approach is employed. Initially, the CNN is pre-trained on simulated data, allowing it to grasp the fundamental dynamics of iron loss. Subsequently, the pre-trained CNN undergoes fine-tuning with a carefully selected, albeit limited, set of experimental data. This refinement is guided by a

carefully defined loss function, ensuring that the model can better adapt and generalise to real-world scenarios despite the constraints posed by the availability of experimental data. Ultimately, experimental validation underscores the substantial benefits offered by this hybrid mechanism-data-driven model in iron loss modelling. By seamlessly blending the predictive capabilities of deep learning with the physical insights garnered from traditional methods, it enhances the accuracy and efficiency of iron loss predictions while also pioneering new paths for tackling complex physical challenges.

The remainder of this paper is organised as follows. Section 2 introduces the overall framework of the hybrid mechanism-data-driven modelling approach, which consists of three phases. The enhanced iron loss analysis model that considers multidisciplinary influencing factors is analysed and presented as well. Section 3 illustrates the methodology for deep learning and fine-tuning optimisation using the CNN model. In Section 4, a hybrid mechanism-data-driven iron loss model for an interior permanent magnet synchronous motor (IPMSM) used in electric vehicles (EVs) is developed. Then, the test system is utilised for the case studies to validate the effectiveness of the proposed model. The conclusions of the research are given in Section 5.

2 | PROBLEM FORMULA AND MODELS

2.1 | Framework of the proposed modelling method

The comprehensive illustration of the proposed hybrid mechanism-data-driven modelling method for iron loss prediction, as depicted in Figure 1, encapsulates a three-stage methodology. The initial stage integrates a mechanistic analytical approach to iron loss modelling with CNNs for deep learning. This phase is designed to establish a foundational physics-informed data-driven deep learning model. The critical elements encompassed are given as follows.

(1) Leveraging the Simplorer and Ansys software, the PWM-induced magnetic flux density, temperature and mechanical stress profiles can be generated across diverse loading conditions and frequencies. It should be noted that using the discrete Fourier transform, the magnitudes of fundamental components and individual harmonics of the airgap flux density can be calculated, and then the airgap flux density waveforms under both sinusoidal and PWM supplies were obtained through combined simulations of Simplorer and ANSYS. These profiles, along with an enhanced iron loss analysis model that integrates hysteresis and eddy current loss constants tailored to the specific iron core materials, and further adjusts for temperature increases and mechanical stresses, produce datasets of iron losses under various operational conditions. The method meticulously captures the intricate, multidisciplinary-driven dynamics of iron losses.

(2) Based on the iron loss data, the CNN model is trained to learn and represent the diverse range of characteristics associated with the iron loss process. A tailored loss function is employed during the training to quantify the discrepancy between predicted and observed iron loss values, thereby guiding the backpropagation algorithm and gradient adjustments. The iterative refinement process would greatly improve the CNN's predictive capability and accuracy.

(3) The culmination of this hybrid mechanism-data-driven modelling approach lies in its application domain. The devised model can be deployed for extensive simulation scenarios pertaining to PMSMs. Moreover, the generality of the proposed modelling strategy transcends PMSMs, rendering it applicable to a diverse array of motor types and beyond, for various types of loss modelling endeavours. This underscores the model's potential to serve as a versatile tool for comprehensive loss analysis across diverse electromechanical systems.

2.2 | Mechanism-based iron loss analytical model

The proposed mechanism-based iron loss analytical models address both the spatial harmonics caused by stator slotting

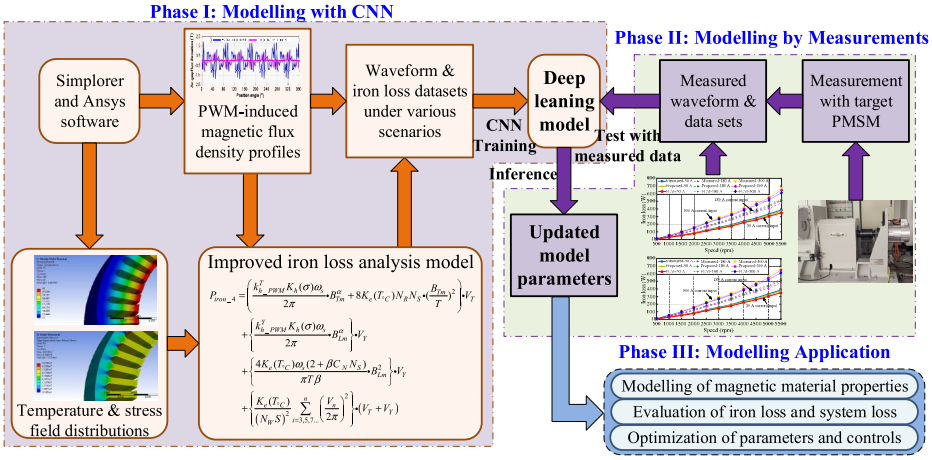

FIGURE 1 Framework of the proposed hybrid mechanism-data-driven modelling methods.

and carrier harmonics resulting from pulse width modulation (PWM) inverter. The models also predict iron loss in tooth and yoke regions separately, taking into account the impacts of magnetic saturation, temperature rising and mechanical stress. It should be noted that the excess loss in PMSMs, influenced by factors difficult to model such as motor geometry and operational conditions, is neglected in the iron loss calculations due to its small impacts, ensuring simplicity and practicality.

As described in our previous publication [3], to deal with the influence of slot harmonics, flux density is transformed into a trapezoidal waveform by FEM, then the iron loss densities in tooth and yoke regions can be calculated using the following equation:

$$\begin{cases} P_{totalT} = K_h \dfrac{\omega_s}{2\pi} B_{Tm}^{\alpha} + 8K_e \cdot N_R N_S \left(\dfrac{B_{Tm}}{T}\right)^2 \\ P_{totalY} = K_h \dfrac{\omega_s}{2\pi} B_{Lm}^{\alpha} + 8K_e \cdot \dfrac{\omega_s B_{Lm}^2}{\pi\beta T} + C_N \cdot 4K_e \dfrac{N_S \omega_s}{\pi T} B_{Lm}^2 \end{cases} \tag{1}$$

And the total iron loss in the stator core considering spatial harmonics is determined with the following equation:

$$P_{iron\_1} = P_{totalT} V_T + P_{totalY} V_Y \tag{2}$$

The meanings of symbols are referred to the nomenclature at the beginning of the paper.

While the iron loss model presented in Equations (1) and (2) considers the impact of magnetic field distribution and spatial harmonics, it was developed with the presumption that the motor is driven by sinusoidal current inputs. In practice, PMSMs are typically driven by inverters with control circuits that operate over a wide range of speeds and torques, generating additional iron loss from carrier harmonics.

Thus, a refined model is employed to consider the impact of PWM carrier harmonics on the iron loss computation. This model defines a modified coefficient k_{h_PWM}, which adjusts the calculation equations for hysteresis loss. Moreover, the eddy current loss model is replaced to incorporate the cumulative effect of all the components caused by the harmonics [26].

$$\begin{cases} P_{h\_PWM} = k_{h\_PWM} P_h \\ P_{e\_PWM} = \sum P_{e\_PWM}(n) \end{cases} \tag{3}$$

where

$$k_{h\_PWM} = 1 + C_h \frac{1}{B_m} \sum_{a=1}^{N} \Delta B_a \tag{4}$$

Assuming that the PWM inverter's output voltage is a periodic function, which can be expressed via Equation (5) using the Fourier series [27],

$$v(t) = V_1 \cos 2\pi f t + \sum_{n=3,5,7,\cdots}^{\infty} V_n \cos 2n\pi f t \tag{5}$$

Then, based on the Faraday's law, the magnetic flux density considering carrier harmonics can be expressed as follows:

$$B(t) = \frac{1}{N_W S}\left(\sum_{n=1\ ,\ 3,5,\ldots}^{\infty} \frac{V_n}{2n\pi f} \sin 2n\pi f t\right) \tag{6}$$

The magnitude of the nth harmonic of flux density is given as follows [28]:

$$B_{mn} = \frac{1}{N_W S} \cdot \frac{V_n}{2n\pi f} \tag{7}$$

Using the Bertotti method, $P_{e\_PWM}(n)$ can thus be obtained via the following equation:

$$\begin{aligned} P_{e\_PWM}(n) &= K_e B_{mn}^2 f_n^2 \\ &= K_e \left(\frac{1}{N_W S} \cdot \frac{V_n}{2n\pi f}\right)^2 f_n^2 = K_e \left(\frac{1}{2\pi N_W S}\right)^2 V_n^2 \end{aligned} \tag{8}$$

Combining Equations (1), (2), (3), (4) and (8), the iron loss model considering both spatial and PWM harmonics is updated via the following equation:

$$\begin{aligned} P_{iron\_2} = &\left(k_{h\_PWM}^T P_{hT} + P_{eT}\right) V_T \\ &+ \left(k_{h\_PWM}^Y P_{hY} + P_{eYL} + P_{eYN}\right) V_Y \\ &+ \left[K_e \left(\frac{1}{N_W S}\right)^2 \cdot \sum_{i=3,5,7\ldots}^{n} \left(\frac{V_n}{2\pi}\right)^2\right] \cdot (V_T + V_Y) \end{aligned} \tag{9}$$

Given the temperature sensitivity of core materials, it is imperative to incorporate the effects of temperature fluctuations into iron loss calculations. Furthermore, the residual stress within silicon steel sheets, stemming from processes such as punching, cutting, and pressing, constitutes a significant contributor to performance deterioration. This residual stress triggers a reorganisation of internal magnetic domains, subsequently augmenting iron loss, a phenomenon that underscores the necessity of addressing these stress factors in iron loss modelling.

To account for the thermal and mechanical stress effects, the iron loss coefficients K_h and K_e are both defined as functions of working temperature $T_{\circ C}$ and mechanical stress σ. As a result, the final iron loss model considering coupling effects can be updated using the following equation:

$$P_{iron\_3} = \left(\frac{k_{h\_PWM}^{T} K_h(T_{\circ C}, \sigma) \cdot \omega_s}{2\pi} \cdot B_{Tm}^{\alpha} + 8K_e(T_{\circ C}, \sigma) N_R N_S \cdot \left(\frac{B_{Lm}}{T}\right)^2\right) \cdot V_T + \left\{\frac{k_{h\_PWM}^{Y} K_h(T_{\circ C}, \sigma) \cdot \omega_s}{2\pi} \cdot B_{Lm}^{\alpha} + \frac{4K_e(T_{\circ C}, \sigma) \cdot \omega_s (2 + \beta C_N N_S)}{\pi T \beta} \cdot B_{Lm}^{2}\right\} \cdot V_Y + \left\{\frac{K_e(T_{\circ C}, \sigma)}{(N_W S)^2} \sum_{i=3,5,7\ldots}^{n} \left(\frac{V_n}{2\pi}\right)^2\right\} \cdot (V_T + V_Y) \tag{10}$$

2.3 | Correlation analysis

To streamline the calibration of iron loss coefficients, the Pearson correlation analysis approach is utilised to delve into the interplay between loss coefficients and various multiphysics factors. Specifically, the Pearson correlation coefficient, denoted as R_{XY}, is defined in a manner that quantifies the strength and direction of the linear relationships between the coefficients and the influencing factors, thereby facilitating a more efficient and insightful fitting process [29].

$$R_{XY} = \frac{\sum_{i=1}^{n} (X_i - \overline{\mathbf{X}})(Y_i - \overline{\mathbf{Y}})}{\sqrt{\sum_{i=1}^{n} (X_i - \overline{\mathbf{X}})^2} \cdot \sqrt{\sum_{i=1}^{n} (Y_i - \overline{\mathbf{Y}})^2}} \tag{11}$$

Furthermore, the magnitude of R_{XY} approaching unity signifies a robust correlation between the input and output variables. Employing comprehensive FEM data, the Pearson correlation indices that link the iron loss coefficients are derived based on the multifaceted physical data across a broad range of operational speeds, spanning from 500 to 5500 rpm, as presented in Figure 2.

As seen, it is evident that the hysteresis loss coefficient exhibits a pronounced correlation with stress levels, whereas the eddy current loss coefficient is notably influenced by temperature variations. As a result, the derived iron loss model in Equation (10) can finally be refined via the following equation:

$$P_{iron\_2} = \left(\frac{k_{h\_PWM}^{T} K_h(\sigma) \omega_s}{2\pi} \cdot B_{Tm}^{\alpha} + 8K_e(T_{\circ C}) N_R N_S \cdot \left(\frac{B_{Tm}}{T}\right)^2\right) \cdot V_T + \left\{\frac{k_{h\_PWM}^{Y} K_h(\sigma) \omega_s}{2\pi} \cdot B_{Lm}^{\alpha}\right\} \cdot V_Y + \left\{\frac{4K_e(T_{\circ C}) \omega_s (2 + \beta C_N N_S)}{\pi T \beta} \cdot B_{Lm}^{2}\right\} \cdot V_Y + \left\{\frac{K_e(T_{\circ C})}{(N_W S)^2} \sum_{i=3,5,7\ldots}^{n} \left(\frac{V_n}{2\pi}\right)^2\right\} \cdot (V_T + V_Y) \tag{12}$$

where $K_h(\sigma)$ and $K_e(T_{\circ C})$ can be acquired by fitting the iron loss curves obtained from experimental measurements of silicon steel sheets under various frequencies, temperatures and stresses, using a 2D magnetic properties tester [30].

3 | HYBRID MECHANISM-DATA-DRIVEN IRON LOSS MODEL BASED ON CNN

Neural networks, through learning and training on data, can effectively approximate complex non-linear mapping relationships. They store all quantitative or qualitative information distributed across the neurons within the network. This enables them to perform rapid and large-scale computations and to provide online inference speeds, meeting real-time requirements. The CNNs can effectively reduce network complexity and decrease the number of training parameters. They possess strong robustness and fault tolerance, making them easy to implement training and optimisations. Therefore, this paper selects CNN, which includes input layer, convolutional layer, activation

functions, pooling layer, fully connected layer, and output layer, as the data-driven modelling approach. The topology of the used CNN is presented as Figure 3.

Based on the prediction model for iron losses in IPMSMs, six key features are selected as inputs to the CNN, namely the load currents, working temperature, mechanical stress, mechanical speed, tooth magnetic flux density, and the yoke magnetic flux density. These parameters were chosen due to their direct relationships with electromagnetic forces, material properties, microstructural changes in the iron core, and harmonic content of the magnetic field, all of which significantly contribute to iron losses and require accurate prediction for optimal motor performances. The input layer of CNN comprises a one-dimensional vector of size 1×6, such that a one-dimensional convolutional kernel is employed in this paper considering that they can not only well process one-dimensional data vectors, but also achieve the fusion of multiple feature maps. The convolutional layer performs local connections and weighted bias operations between the convolutional kernel and the feature map from the previous layer, and then passes the results to the activation function to obtain feature maps. The weights of the same convolutional kernel are shared, and multiple convolutional kernels are used to obtain multi-layer feature maps.

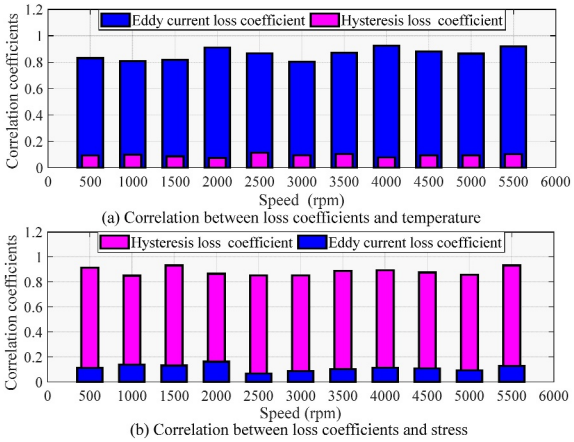

FIGURE 2 Correlations between K_h and K_e with working temperature and mechanical stress.

$$y_j^h = g\left(\sum_{i=1}^{N_k} m_i^{h-1} * k_{ij}^h + b_j^h\right) \tag{13}$$

The activation function is used to enhance the non-linear mapping of the convolutional kernel output. In CNNs, the ReLU function is typically used as the activation function, which operates as follows.

$$g(h) = \begin{cases} h, & h > 0 \\ 0, & h \le 0 \end{cases} \tag{14}$$

To fully extract the feature information, this paper employs two convolutional layers. The parameters of these layers are given in Table 1.

The pooling layer, typically aimed at reducing the resolution of feature maps to attain spatial invariance crucial for image recognition tasks, is intentionally omitted in this paper. Instead, the fully connected layer is employed to integrate the diverse feature maps extracted by the convolutional layers. The configuration of this fully connected layer is detailed as follows:

$$y^h = g\left(m^{h-1} \times \boldsymbol{\omega}^h + b^h\right) \tag{15}$$

The output of the fully connected layer is converted into a probability distribution through Softmax logistic regression for classification and final output. In this paper, the fully connected layer configuration of (64, 80, 1) is employed. The output of the network's output layer signifies the predicted iron loss as determined by the neural network. Eq. (9) depicts the loss function of the devised CNN, which characterises the optimisation efficacy and objectives of the network model.

$$\mathrm{RMSE} = \sqrt{\frac{1}{N}\sum_{i=1}^{N}(\hat{y}_i - y_i)^2} \tag{16}$$

CNN training encompasses two iterative processes: forward inference and error backpropagation. During forward propagation, the network computes predictions which are then compared with the ground truth values to calculate the loss error. This error, in turn, is utilised to compute the gradients for each parameter. Subsequently, the Adam optimiser, with a

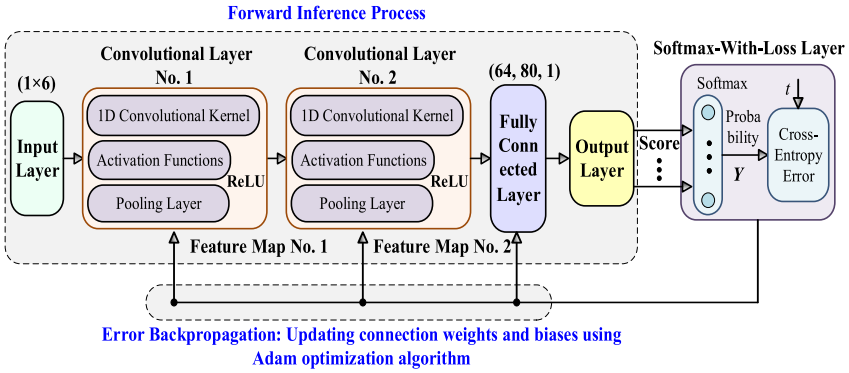

FIGURE 3 Topology structure of the used CNN.

TABLE 1 Convolutional layer parameters.

Parameters	Conv1	Conv2
Number of convolutional kernels	16	32
Kernel size	2	2
Convolutional stride	2	1

learning rate of 0.001, is employed to update the network parameters including connection weights and biases in both convolutional and fully connected layers. By iteratively repeating these steps, the network parameters are continuously adjusted, gradually refining the mapping relationship between inputs and outputs.

4 | CASE STUDIES

In this paper, MATLAB is used as a simulation tool to conduct the experiments while Ubuntu 16.04 with Python 3.6 and TensorFlow 1.5 is employed as the deep learning framework. The computer configuration used for the experiments includes an Intel Core i7 1185G7 processor at 3 GHz with 16 GB of memory. The co-simulation of Simplorer and Ansys runs on a Linux-based high-performance computing cluster, which features 56 CPU cores and up to 1.5 TB of memory per node. This setup is well-suited for handling large bioinformatics datasets, complex physical simulations, and multidimensional datasets.

The training data is obtained offline. Given the importance of multidisciplinary coupled modelling, six input variables were carefully selected from the thresholds of their respective domains. These variables are essential for simulating and calculating iron loss for subsequent training data. Through the aforementioned simulations and experiments, a total of 5000 sets of training data, each comprising 6 inputs and 1 output, were obtained. Because the training set drives the CNN model's learning process, and the testing data is crucial for assessing the model's prediction accuracy in actual operations, measuring a 14% ratio to the testing set necessitates the procurement of an additional 700 data points specifically tailored to evaluate the predictive performances of the iron loss model. Incorporating actual measurement data into the testing set significantly enhances the model's authenticity, generalisation capabilities, and robustness. Given the minor influences of stator temperature and motor stress on the speed's rate of change, the primary variations in measured data are primarily dictated by speed and load currents, with each of these variables contributing around 24 instances to the testing data set.

The experimental data is measured employing a self-developed IPMSM prototype, equipped with the conventional sinusoidal PWM. A field-oriented control (FOC) strategy ($I_d = 0$) [31] is utilised to conduct the experiments, aiming to achieve the maximum torque per ampere, in which the current and speed loops are set as feedback loops to keep the reference speed as well as to make a minimal d-axis reference current. The key specifications are presented in Table 2. The FEM model of the prototype as well as the diagram of the integrated

TABLE 2 Specifications of the IPMSM prototype used in EVs.

Items	Values	Items	Values
No. of poles	8	Core material	35WW360
No. of slots	48	Core length	108 mm
No. of phases	3	Stator outer diameter	196 mm
Magnets per pole	2	Stator inner diameter	135 mm
Rated power	20 kW	Rotor outer diameter	134 mm
Rated speed	3600 rpm	Air-gap length	0.5 mm
Maximum power	40 kW	Tooth width	6.35 mm
Maximum speed	5500 rpm	Magnet width	19.5 mm
Rated torque	53 Nm	V-shaped angle	145°
Maximum torque	180 Nm	Phase resistance	0.0052 Ω

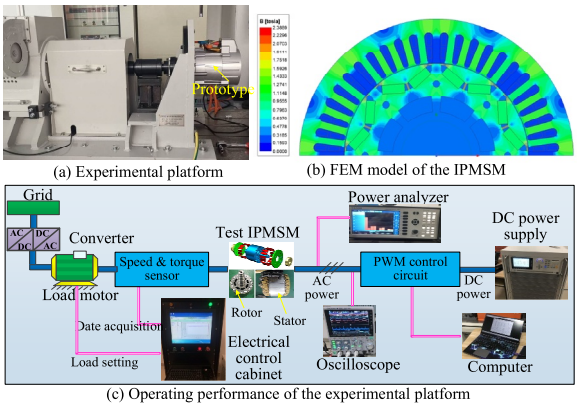

(a) Experimental platform (b) FEM model of the IPMSM

(c) Operating performance of the experimental platform

FIGURE 4 Setup of the FEM model and integrated experimental platform.

experimental platform are both given in Figure 4. As shown, the control and measuring equipment are mounted on the experimental platform, including the control and drive circuits, the dynamometer, and the dynamic torque/speed sensors. The DC power supply is used for providing the desired DC power to the testing motor, the upper computer is used for writing the control programme, and the electrical control cabinet can be employed to simulate different load conditions, while the oscilloscope is applied for the data recording.

The offline training results of the CNN network, respectively using the training and texting date, are presented as Figure 5. It is indicated that the loss function, namely the RMESs of the output variable stops decreasing after around 1700 iterations. During this period, each parameter of the CNN network reaches its optimal values through the utilisation of backpropagation and gradient descent on the training parameters.

Through the built experimental platform, the actual iron losses are obtained under various speed and load conditions, and then compared with the values predicted using the presented CNN model. To accurately determine the iron loss values, a so-called dummy rotor method [32] was employed to obtain the mechanical losses, which can be calculated as the input power of the drive motor since there is no rotor magnet, hence no iron loss

or induced current & copper loss. The results are illustrated as Figure 6, in which the blue '*' symbols indicate the actual iron loss of the motor, while the magenta '.' symbols represent the iron loss values predicted by the proposed network model. The different colours, that is, orange, blue, and purple, represent different load conditions. By comparing the predicted values with the actual iron loss values, the scatter plot shows a good overlap between the two types of symbols.

The error analysis results are summarised in Figure 7. As shown in Figure 7a, the normalised residuals between the predicted and actual iron loss are quite small under various operating conditions. Given Figure 7b, the kurtosis of both the histogram and kernel density are pretty high, accounting for about 0.22 where the residual is approximately zero, indicating that the residuals are concentrated. Although the kernel density shows a slight fluctuation, the residual distribution closely aligns with a normal distribution, validating the robust predictive ability of the proposed iron loss model. According to the box plot of Figure 7c, the maximum and minimum residuals are calculated as 5.59% and −5.29%, respectively, while the median is around 0.13% with the 25th percentile as −1.22% and the 75th percentile as 1.55%. Results indicate that the proposed hybrid mechanism-data-driven model can effectively predict the iron loss of PMSMs with satisfactory accuracy and stability.

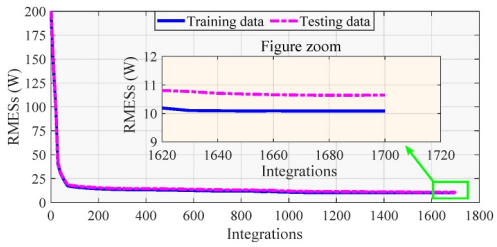

FIGURE 5 Offline training results of the CNN-based loss model.

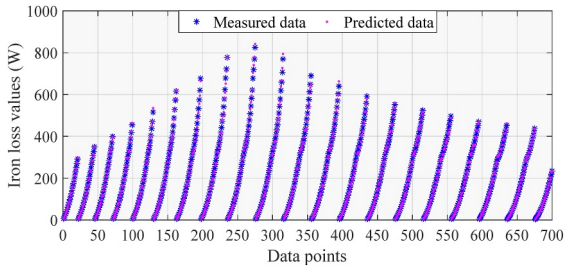

FIGURE 6 Validating results of the iron loss model predicted using the proposed hybrid CNN approaches.

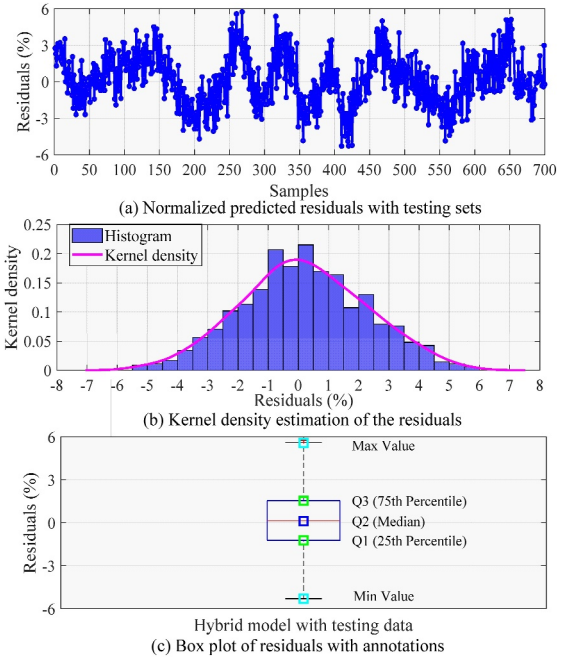

FIGURE 7 Error analysis of the predicted results.

To further verify the superiority of the proposed approaches, the measured iron losses of the IPMSM prototype are also compared with those predicted using the presented hybrid data-driven model, a traditional CNN model and the advanced analytical iron loss model in [3], under six different current inputs. The comparative results are all presented in Figure 8, while the comparative errors are recorded as Figure 9. The data analysis of Figures 8 and 9 are all collected in Table 3, where *EMj* and *EAj* (j = 32, 90, 180, 285, 400 and 490) represent the maximum and absolute average errors of iron losses which are relative to the measured data under 32, 90, 180, 285, 400 and 588 A phase currents, respectively.

As shown in Figure 8, the proposed hybrid mechanism-data-driven model shows outstanding performance for predicting the iron loss of the IPMSM prototype. Under different working speeds and various current inputs, the predicted iron loss curve is closest to the measured values, compared to those obtained through the traditional CNN model and the advanced analytical iron loss model. The accuracy and stability are also satisfactory.

As shown in Figure 9, the iron loss models developed using traditional CNN and the improved analytical method respectively have the maximum errors as −7.12% and −5.46% under all six different input phase currents, while the maximum error using the proposed hybrid data-driven approach obtains only −4.98% for 400 A input current. The values of maximum errors for the other five input currents are all less than 4%. Moreover, the predicting accuracy stability of the proposed method also outperforms the other models. Under different working conditions, the absolute average error of the iron loss predicting using the proposed model is all within 2.11%, which is only around half of the values by traditional CNN and 70% of those obtained with the improved analytical in [3]. All the results well-verify the satisfactory performances of the proposed hybrid mechanism-data-driven iron loss model under various working conditions.

5 | CONCLUSION

Considering the difficulty in all the data acquisition, the complexity of physical models, and the highly coupled multi-disciplinary influencing factors for iron loss prediction of

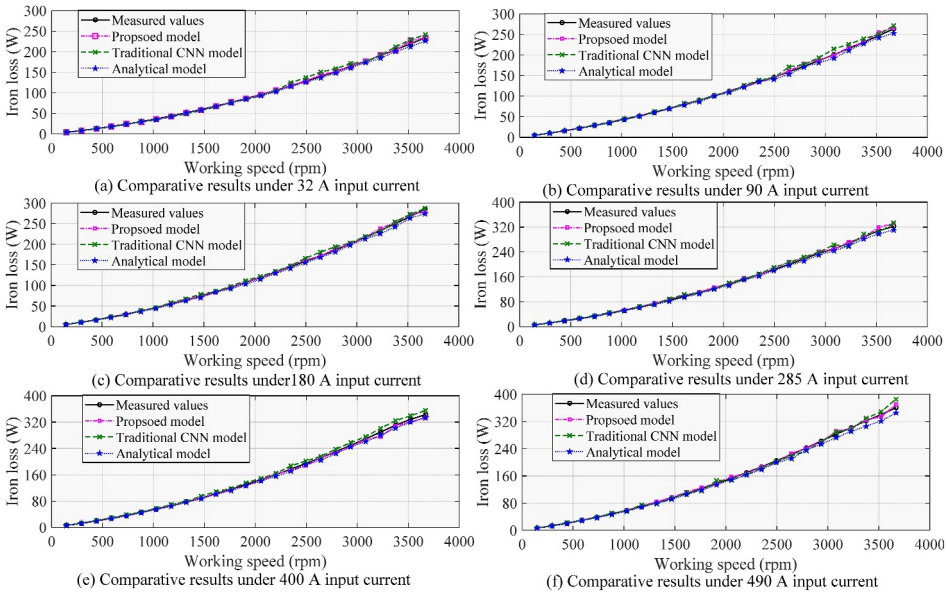

FIGURE 8 Comparative results of iron loss models.

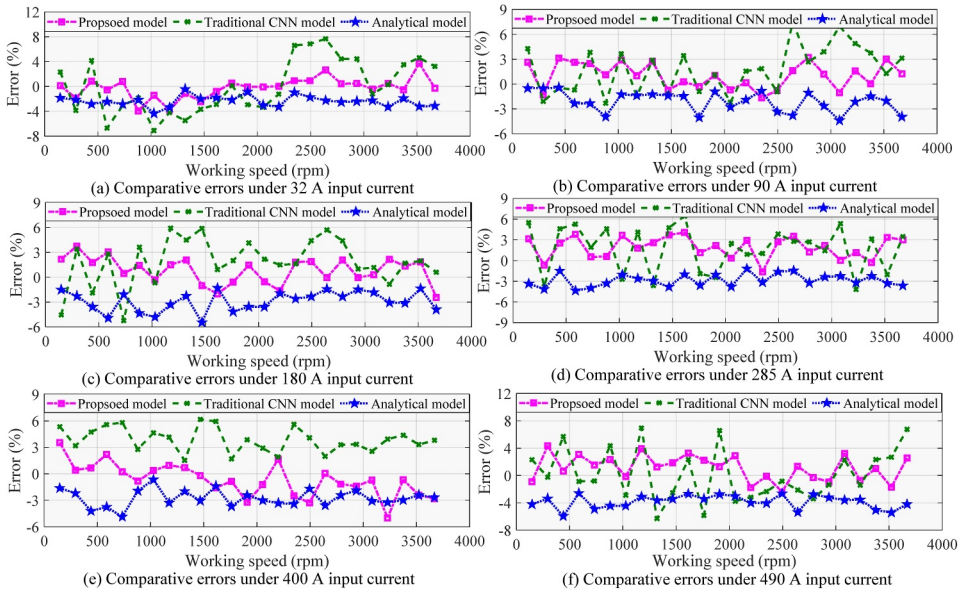

FIGURE 9 Error analysis of the comparative results.

TABLE 3 Data analysis of Figures 8 and 9.

Items	Proposed	Traditional CNN	Analytical model	Items	Proposed	Traditional CNN	Analytical model
EM_{32}	−3.92%	−7.12%	−3.35%	EM_{285}	3.78%	6.45%	−4.36%
EA_{32}	1.17%	3.84%	2.67%	EA_{285}	2.11%	3.39%	2.85%
EM_{90}	3.21%	4.95%	−4.38%	EM_{400}	−4.98%	6.18%	−4.86%
EA_{90}	1.54%	2.50%	2.08%	EA_{400}	1.55%	3.86%	2.75%
EM_{180}	3.76%	2.76%	−5.46%	EM_{490}	3.95%	6.95%	−5.43%
EA_{180}	1.52%	2.91%	2.90%	EA_{490}	1.83%	3.21%	3.84%

electrical machines, this paper proposes a hybrid mechanism-data-driven model that combines both physical and AI approaches for accurate estimation of iron loss. The physical model provides the foundational theories and constraints, while the data-driven model is used to capture complex nonlinear and unmodeled dynamic characteristics. The accuracy

of this integrated method is rigorously validated through randomised operating condition tests on an IPMSM prototype. The key conclusions can be summarised as follows.

(1) Statistical analysis revealed a median residual of 0.13% with a tight range, where the 75th percentile fell within only ±1.55% of actual values. The maximum and minimum residuals are also acceptable, highlighting the hybrid model's capacity for high-precision predictions.
(2) With different input currents and working speeds, the absolute average error across all conditions remained below 2.11%, around half that of traditional CNN and 70% of improved analytical methods, demonstrating the model's robust stability and reliability.

These numerical achievements validate the proposed hybrid model's ability to accurately and consistently predict iron losses in electrical machines, setting a new benchmark for high-precision dynamic predictions amidst complex operational scenarios. The success of this study underscores the potential of combining physical insights with advanced data-driven techniques to tackle complex engineering challenges, paving the way for future advancements in motor design and performance optimisation.

AUTHOR CONTRIBUTIONS

Lin Liu: Formal analysis; Methodology; Writing - original draft. **Wenliang Yin**: Methodology; Resources; Software; Writing - review & editing. **Youguang Guo**: Conceptualisation; Funding acquisition; Supervision.

ACKNOWLEDGEMENT

This work is supported by the National Natural Science Foundation of China under grant 52005306, Australian Research Council under Discovery Grants DP120104305 and DP180100470, and the Foundation of China Scholarship Council under Grant 201906730038. Open access publishing facilitated by University of Technology Sydney, as part of the Wiley - University of Technology Sydney agreement via the Council of Australian University Librarians.

NOMENCLATURE

K_h, K_e	Empirical hysteresis and eddy current loss coefficients
B_{TM}, B_{LM}	Amplitude of magnetic flux density in tooth and yoke regions
N_R, N_S	Numbers of phases and slots per pole per phase
V_T, V_Y	Volumes of tooth and yoke
ω_S, T	Motor angular frequency and excitation period
α, C_N	Empirical coefficients and derived fitting coefficients
P_h, B_m	Hysteresis loss density and Amplitude of magnetic flux density
ΔB_a	Fluctuation in motor flux density
f, f_n	Fundamental and nth harmonic frequencies of PWM waveform
$P_{e\_PWM}(n)$	Eddy current loss caused by the nth PWM harmonic
V_n	Magnitude of the nth harmonic voltage
N_W, S	Number of winding turns, and cross-sectional area of iron core
P_{hT}, P_{hY}	Hysteresis loss density in the tooth and yoke regions
P_{eT}, P_{eY}	Eddy current loss density in the tooth and yoke regions
P_{eYL}, P_{eYN}	P_{eY} with longitudinal flux and normal component
$T_{°C}$, σ	Working temperature and mechanical stress
R_{XY}	Pearson correlation coefficient
X	$X = \{X_i;\ i = 1, \cdots N\}$, the set of input variables
Y	$Y = \{Y_i;\ i = 1, \cdots N\}$, the set of corresponding output variables
$\overline{X}$, $\overline{Y}$	Means of X and Y
y_j^h	Output of the jth feature map at the hth layer
$g(x)$	Activation function
N_k	Number of feature maps output by the (h-1)th layer
m_i^{h-1}	The ith feature map output by the (h-1)th layer
$*$	Convolution operation
k_{ij}^h	The jth convolution kernel for the current hth layer
b_j^h	Bias for k_{ij}^h
$\boldsymbol{\omega}^h$	Weight matrix of the hth layer
N	Number of the samples
$\hat{y}_i$	Predicted values of the output

CONFLICT OF INTEREST STATEMENT

The authors declare no conflicts of interest.

DATA AVAILABILITY STATEMENT

Authors elect to not share data.

ORCID

Lin Liu https://orcid.org/0000-0003-1190-6249
Wenliang Yin https://orcid.org/0000-0002-4288-8031

REFERENCES

1. Ruuskanen, V., et al.: Iron loss analysis of the permanent-magnet synchronous machine based on finite-element analysis over the electrical vehicle drive cycle. IEEE Trans. Ind. Electron. 63(7), 4129–4136 (2016). https://doi.org/10.1109/tie.2016.2549005
2. Yin, W., et al.: Self-stabilising speed regulating differential mechanism for continuously variable speed wind power generation system. IET Renew. Power Gener. 14(15), 3002–3009 (2020). https://doi.org/10.1049/iet-rpg.2019.1407
3. Liu, L., et al.: Improved iron loss prediction models for interior PMSMs considering coupling effects of multiphysics factors. IEEE Trans. Transp. Electrific. 9(1), 416–427 (2023). https://doi.org/10.1109/tte.2022.3189504
4. Chen, X., et al.: A high-fidelity and computationally efficient model for interior permanent-magnet machines considering the magnetic saturation, spatial harmonics, and iron loss effect. IEEE Trans. Ind. Electron. 62(7), 4044–4055 (2015). https://doi.org/10.1109/tie.2014.2388200

5. Bertotti, G., et al.: An improved estimation of iron losses in rotating electrical machines. IEEE Trans. Magn. 27(6), 5007–5009 (1991). https://doi.org/10.1109/20.278722
6. Zhao, X., et al.: A dynamic hysteresis model for loss estimation of GO silicon steel under DC-biased magnetization. IEEE Trans. Ind. Appl. 57(1), 409–416 (2021). https://doi.org/10.1109/tia.2020.3038712
7. Minowa, N., Takahashi, Y., Fujiwara, K.: Iron loss analysis of interior permanent magnet synchronous motors using dynamic hysteresis model represented by cauer circuit. IEEE Trans. Magn. 55(6), 1–4 (2019). https://doi.org/10.1109/tmag.2019.2902428
8. Patsios, C., et al.: Dynamic finite element hysteresis model for iron loss calculation in non-oriented grain iron laminations under PWM excitation. IEEE Trans. Magn. 47(5), 1130–1133 (2011). https://doi.org/10.1109/tmag.2010.2073690
9. Shi, Z., et al.: Design optimisation of an outer-rotor permanent magnet synchronous hub motor for a low-speed campus patrol EV. IET Electr. Power Appl. 14(11), 2111–2118 (2020). https://doi.org/10.1049/iet-epa.2020.0130
10. Ge, B., et al.: Research on loss differences and thermal optimisation of submerged cryogenic high-speed permanent magnet motors. IET Electr. Power Appl. 18(11), 1554–1566 (2024). https://doi.org/10.1049/elp2.124
11. Kowal, D., et al.: Comparison of iron loss models for electrical machines with different frequency domain and time domain methods for excess loss prediction. IEEE Trans. Magn. 51(1), 1–10 (2015). https://doi.org/10.1109/tmag.2014.2338836
12. Zhu, S., Shi, B.: Modeling of PWM-induced iron losses with frequency-domain methods and low-frequency parameters. IEEE Trans. Ind. Electron. 69(3), 2402–2413 (2022). https://doi.org/10.1109/tie.2021.3065626
13. Xue, S., et al.: A new iron loss model for temperature dependencies of hysteresis and eddy current losses in electrical machines. IEEE Trans. Magn. 54(1), 1–10 (2018). https://doi.org/10.1109/tmag.2017.2755593
14. Kulan, M.C., et al.: Empirical implementation of the steinmetz equation to compute eddy current loss in soft magnetic composite components. IEEE Access 10, 14610–14623 (2022). https://doi.org/10.1109/access.2022.3148593
15. Mahmud, M., et al.: Applications of deep learning and reinforcement learning to biological data. IEEE Transact. Neural Networks Learn. Syst. 29(6), 2063–2079 (2018). https://doi.org/10.1109/tnnls.2018.2790388
16. Wang, Y., et al.: Hybrid electric vehicle energy management with computer vision and deep reinforcement learning. IEEE Trans. Ind. Inf. 17(6), 3857–3868 (2021). https://doi.org/10.1109/tii.2020.3015748
17. Li, Y., et al.: Systematic evaluation of deep neural network based dynamic modeling method for AC power electronic system. CES Trans. Electr. Mach. Syst. 7(2), 137–143 (2023). https://doi.org/10.30941/cestems.2023.00011
18. Chen, S., et al.: Complex-valued B-spline neural networks for modeling and inverting hammerstein systems. IEEE Transact. Neural Networks Learn. Syst. 25(9), 1673–1685 (2014). https://doi.org/10.1109/tnnls.2014.2298535
19. Zhao, Z., et al.: Physics informed neural network-based high-frequency modeling of induction motors. Chin. J. Electr. Eng. 8(4), 30–38 (2022). https://doi.org/10.23919/cjee.2022.000036
20. Kirchgässner, W., Wallscheid, O., Böcker, J.: Estimating electric motor temperatures with deep residual machine learning. IEEE Trans. Power Electron. 36(7), 7480–7488 (2021). https://doi.org/10.1109/tpel.2020.3045596
21. Ortombina, L., Tinazzi, F., Zigliotto, M.: Magnetic modeling of synchronous reluctance and internal permanent magnet motors using radial basis function networks. IEEE Trans. Ind. Electron. 65(2), 1140–1148 (2018). https://doi.org/10.1109/tie.2017.2733502
22. Tahkola, M., Mukherjee, V., Keränen, J.: Transient modeling of induction machine using artificial neural network surrogate models. IEEE Trans. Magn. 58(9), 1–4 (2022). https://doi.org/10.1109/tmag.2022.3180176
23. Daroogheh, N., et al.: Prognosis and health monitoring of nonlinear systems using a hybrid scheme through integration of PFs and neural networks. IEEE Trans. Syst. Man Cybern.: Off. Syst. 47(8), 1990–2004 (2017). https://doi.org/10.1109/tsmc.2016.2597272
24. Kayedpour, N., et al.: Wind turbine hybrid physics-based deep learning model for a health monitoring approach considering provision of ancillary services. IEEE Trans. Instrum. Meas. 73, 1–14 (2024). https://doi.org/10.1109/tim.2024.3375416
25. Gao, X., Cai, H., Liu, M.: A hybrid multi-scale attention convolution and aging transformer network for alzheimer's disease diagnosis. IEEE J. Biomed. Health. Inf. 27(7), 3292–3301 (2023). https://doi.org/10.1109/jbhi.2023.3270937
26. Yu, L., et al.: Dual-pulse mode control of a high-speed doubly salient electromagnetic machine for loss reduction and speed range extension. IEEE Trans. Ind. Electron. 67(6), 4391–4401 (2020). https://doi.org/10.1109/tie.2019.2931253
27. Chai, F., et al.: Magnet shape optimization of surface-mounted permanent-magnet motors to reduce harmonic iron losses. IEEE Trans. Magn. 52(7), 1–4 (2016). https://doi.org/10.1109/tmag.2016.2524010
28. Chu, W.Q., et al.: Iron loss calculation in permanent magnet machines under unconventional operations. IEEE Trans. Magn. 50(11), 1–4 (2014). https://doi.org/10.1109/tmag.2014.2317784
29. Liu, L., et al.: Efficient design optimization of PMSM drive systems using improved equivalent-circuit-based loss minimization control. IEEE Trans. Ind. Electron., 1–12 (2024). https://doi.org/10.1109/TIE.2024.3447748
30. Liu, L., et al.: Efficient iron loss estimation of interior PMSMs in electric vehicles: analytical modelling and experimental validation. IEEE Trans. Appl. Supercond. 34(8), 1–5 (2024). https://doi.org/10.1109/tasc.2024.3463260
31. Sun, T., et al.: Integration of FOC with DFVC for interior permanent magnet synchronous machine drives. IEEE Access 8, 97935–97945 (2020). https://doi.org/10.1109/access.2020.2996948
32. Guo, Y., et al.: Core loss calculation for soft magnetic composite electrical machines. IEEE Trans. Magn. 48(11), 3112–3115 (2012). https://doi.org/10.1109/tmag.2012.2197677

How to cite this article: Liu, L., Yin, W., Guo, Y.: Hybrid mechanism-data-driven iron loss modelling for permanent magnet synchronous motors considering multiphysics coupling effects. IET Electr. Power Appl. 1–11 (2024). https://doi.org/10.1049/elp2.12530